

Application of Infrared Thermography in Fault Detection and Preventive Maintenance in Three-Phase Distribution Transformers

Jethro Kimande

Institute of Nuclear Science and
Technology, University of Nairobi
Off Harry Thuku Road,
00100 Nairobi, Kenya

Elijah Mwangi

School of Engineering, University of
Nairobi
Off Harry Thuku Road,
00100 Nairobi, Kenya

Michael Gatari

Institute of Nuclear Science and
Technology, University of Nairobi
Off Harry Thuku Road,
00100 Nairobi, Kenya

ABSTRACT

In a three-phase transformer, irregular temperature variation carries information on the underlying faults. In this paper, a fault detection method for three-phase distribution transformers has been developed to identify the type of fault needed for preventive maintenance. Infrared thermography and image processing techniques, like Otsu thresholding, Canny edge detection, image segmentation, and histogram equalization were used in the enhancement of the thermograms to identify the regions of interest (ROIs) from which temperature data have been extracted. It has been established that temperature variation resulting from local faults like loose cable connections have weak correlation compared to those that emanate from loading effects on a transformer. The proposed method is non-invasive, safer and cheaper compared to the conventional methods.

General Terms

Fault Detection, Non-ionizing Radiation, Image Processing

Keywords

Preventive Maintenance, Infrared Thermography, Non-Destructive testing

1. INTRODUCTION

It is essential that distribution transformers in an electricity grid system function efficiently to ensure a stable, uninterrupted supply of electrical power to the consumer. Furthermore, there is a continuous increase in demand for electricity as a result of a considerable number of smart appliances on the consumer side. The rise in consumer load calls for a reliable diagnostic tool that would access the health and performance of transformers for effective preventive maintenance [1], [2], [3],[4].

In recent years, several algorithms have been proposed in the detection of faults in distribution transformers. For instance, the Dissolved Gas Analysis (DGA) method that is widely used in the detection of the incipient faults in transformers [2]. The DGA method relies on laboratory analysis of the transformer oil properties to establish anomalies. However, the method is invasive, time-consuming and is limited to investigating internal faults of the transformer only. Also, Dos Santos et al. [5] proposed the use of Infrared thermography in the detection of incipient faults in transformers by analyzing the surface temperatures of a transformer. Ding et al [2] used fuzzy logic and artificial neural networks in the determination of slow-developing faults, each with a classification of the correctness of 83% and 86%, respectively. Mlakić et al. [6] improved the analysis of thermal images by employing Deep

Learning as an upgrade of artificial neural networks. The infrared thermography techniques employed, however, did not explore the temperature variation at the fuse boxes as well as the individual phase terminations. The algorithms did not extract temperatures or attempt to identify the actual cause of the temperature fluctuations. Besides, local inherent faults like loose cable connections, were not investigated.

This paper proposes a fault identification method in three-phase transformers that uses infrared thermography and image processing. The image processing is based on Otsu thresholding, Canny edge detection, image segmentation, noise reduction, histogram equalization and feature extraction. The proposed method identifies the type of fault and recommends the necessary preventive measures to avert downtimes. In addition, the method investigates temperature variation on the transformer tank, low voltage connection terminals and the fuse boxes surfaces. The extracted temperatures were analyzed to establish whether the fault is local or distributed. It has also been demonstrated that it is possible to investigate inherent faults besides the incipient ones.

The rest of the paper is organized as follows: section 2 describes the theoretical background of infrared thermography. Section 3 gives an overview of the proposed method, and section 4 presents the results of the proposed method. Finally, the conclusion and future work are outlined in section 5.

2. THEORETICAL BACKGROUND

Infrared thermography uses a thermal camera as a core tool to capture and record the temperature distribution on the surface under inspection onto a thermogram. Consequently, the infrared camera can display these temperature values to show the distribution of the surface temperatures in real-time during the inspection [7]. The captured radiation can be analyzed to retrieve information about the object's sub-surface, which is then used to understand its internal configuration or the faults within the object. In thermography, the sub-surface anomalies are shown as regions where the heat flow is modified due to the irregularities. It forms the basis for the identification of a fault in the equipment or materials.

The infrared cameras could be sensitive to either short-wavelength or long-wavelength infrared radiation [8]. These cameras are equipped with the software that can read and convert the temperature data into a thermal image. Thermal images are stored on either the internal camera storage memory or external disk drive with a unique base filename. One typical file compression format is the Joint Photographic

Experts Group (jpeg) [9]. This image compression does not re-size the image physically but preferably compresses that image data to a smaller size. This compression is necessary for processing large images since compressed images load faster and consume less memory space [1].

Infrared thermography encompasses two broad categories, either passive or active IRT [10]. The passive IRT is used to examine and evaluate objects whose temperatures levels are different from the ambient temperatures, which are usually high. It can be used to monitor heat loss in buildings, power stations and in the mapping of the human skin temperatures. This type of IRT does not require external excitations from the temperature source. The active IRT uses an external excitation source like an optical flash lamp, cold or hot air guns, to disrupt the temperature distributions within a material for effective detection of the thermal contrasts. Both active and passive IRT techniques are useful in the detection of abnormalities in the materials or equipment.

3. PROPOSED METHOD

The adopted methodology is presented in Figure 1. An infrared camera was used to record infrared radiations emitted by the three-phase distribution transformer. The images were stored on the memory card and then imported into the MATLAB platform. The image enhancement was carried out in the following steps.

Step (i): The image was first converted to grayscale using adaptive RGB to grayscale conversion using Equation 1.

$$J(x, y) = [a * R(x, y)] + [b * G(x, y)] + [c * B(x, y)] \quad (1)$$

Where values of a, b, and c represent the weight contribution values assigned to the R, G, and B channels of the input image respectively, during the conversion process. The values x and y represent the indices of the pixels in the image and J is the output grayscale image.

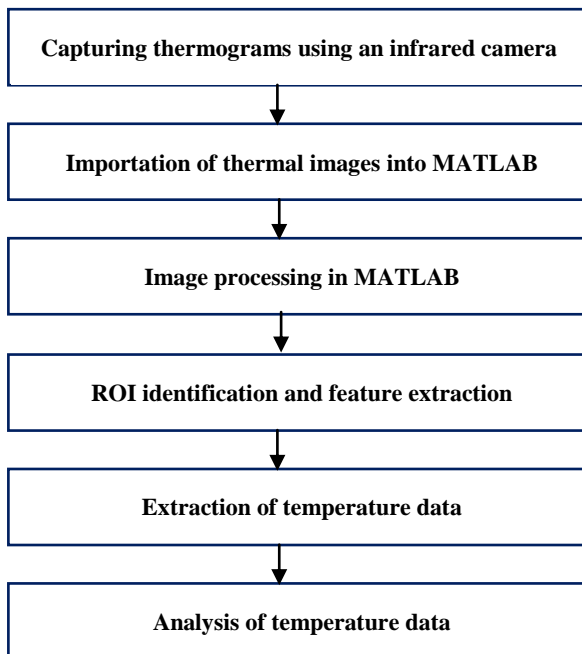


Fig 1: Methodology block diagram

Step (ii): The contrast of the image was enhanced by employing the Adaptive Histogram Equalization with 10 bins and various region tiles with sizes of 10x10, 50x50, 100x100, 150x150 and 200x200 pixels. The number of the bins was

selected to be less than the sum of pixels within the tile size. The image is divided into regions and their histograms evaluated. The image's sectional contrast was then adjusted using the section's local histogram at the provided bin size.

Step (iii): The Canny edge detection was employed in detecting the transformer and fuse box edges. First, the thermograms were smoothed with a Gaussian filter to reduce noise, as given in Equation 2.

$$S(m, n) = \frac{1}{\sqrt{2\pi\sigma^2}} \exp\left[-\frac{m^2 + n^2}{2\sigma^2}\right] \cdot I(m, n) \quad (2)$$

Where the values (m, n) are the pixel coordinates for the input image, σ is the standard deviation, $S(m, n)$ is a value calculated using the Gaussian Kernel formula. and $I(m, n)$ is the input grayscale image.

The gradients of the smoothed image $S(m, n)$ were computed using the 2x2 first difference approximations to produce two arrays $G_x(m, n)$ and $G_y(m, n)$ as in equations 3 and 4.

$$G_x(m, n) = \frac{Smn_1 - S(m, n) + Sm_1n_1 - Sm_1n}{2} \quad (3)$$

$$G_y(m, n) = \frac{S(m, n) - Sm_1n + Smn_1 - Sm_1n_1}{2} \quad (4)$$

Where the expressions $Smn_1 = S(m, n + 1)$, $Sm_1n = S(m + 1, n)$ and $Sm_1n_1 = S(m + 1, n + 1)$.

The magnitude and orientation of the gradient were computed using the standard rectangular-to-polar conversion formulas in equations 5 and 6.

$$|M(m, n)| = \sqrt{G_x^2(m, n) + G_y^2(m, n)} \quad (5)$$

$$\angle M(m, n) = \tan^{-1}\left(\frac{|G_y(m, n)|}{|G_x(m, n)|}\right) \quad (6)$$

Step (iv): Otsu thresholding was performed to convert the image into binary and the image segmentation employed to detect the Regions of Interest (ROIs).

Step (v): Image indexing was performed to map the temperature value on the colourmap to all the identical pixels on the grayscale image. The temperature data was extracted from the ROIs and statistically correlated to identify the type of faults.

4. RESULTS AND DISCUSSION

4.1 Image Enhancement Techniques

The infrared image was obtained using the *Testo 875-2i imager*. Figure 2 shows an example of a thermogram range obtained using the imager from the transformer with tag number G28159. The temperatures on the thermogram ranged between 4 °C to 86.1 °C. The lower temperature values near 4 °C emanated from the pixels in the background, with no defined surface. These pixels are considered to be at the greatest depth of field the *Testo-875i imager* could detect. The image format was Joint Photographic Experts Group file format (.jpeg) with a dimension of 1633x1000 pixels.



Fig 2: Transformer temperature profile

Using the adaptive RGB to grayscale conversion, the average values of each colour channel were computed from their respective centroids. After which the conversion coefficients were computed from the mean intensity values. The resulting image is presented in Figure 3. There was a well-differentiated shade of gray on the colour map on the output image.

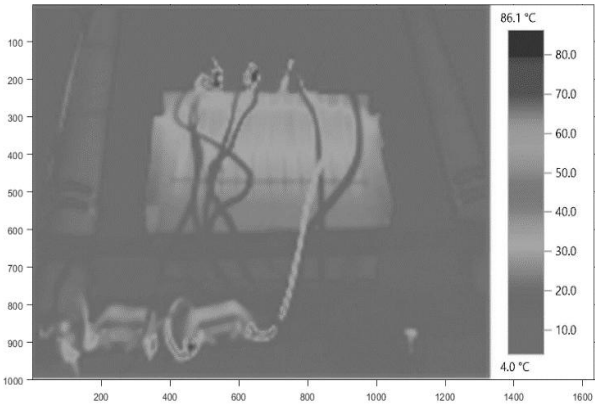


Fig 3: Image output after adaptive RGB to grayscale was applied to the transformer temperature profile

The contrast stretching using Adaptive Histogram equalization (AHE) with a region tile of 200x200 pixels yielded the image in Figure 4. The fuse box and transformer tanks were well contrasted from the background.

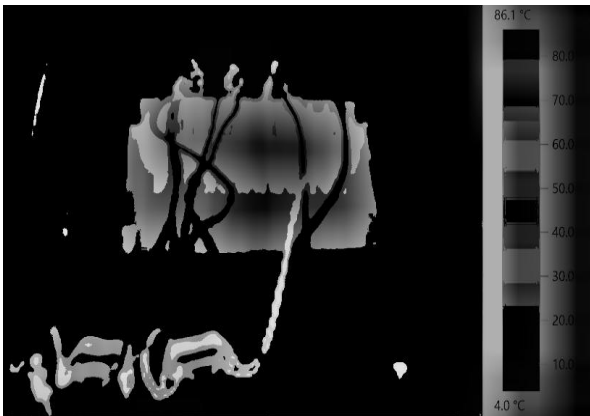


Fig 4: AHE with a window size of 200x200 output image

With a Gaussian mask of 7x7 and variance at 1.96, the edges on the transformer thermogram are visible. The variance was selected as recommended by Gui and Qiwei [11]. At this variance the distorted edges were detected. The image output in Figure 5 shows the edges that are clear and smooth. The transformer and fuse box edges were also visible.

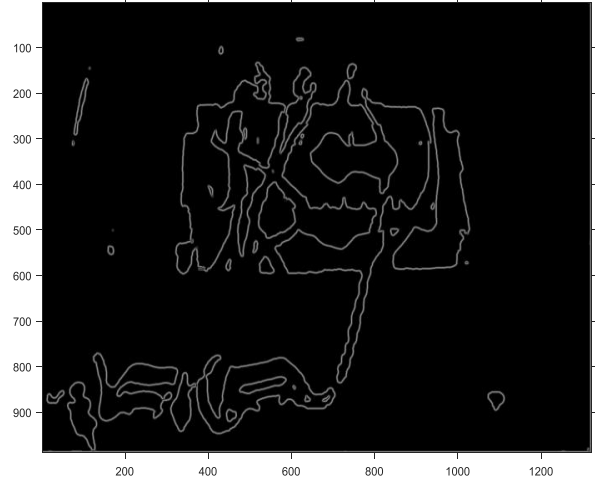


Fig 5: Canny edge detection output

The image segmentation based on Otsu thresholding was performed and the ROIs identified included both the upper and lower parts of the transformer tank and the low voltage fuse section as shown in Figure 6. The low voltage fuse section comprised of several fuse boxes that isolated the 3 voltage phases supplied to the consumers. This fuse arrangement did not follow any order in terms of the phases and varied from transformer to transformer. The temperature data from the ROIs were extracted from 48 thermograms captured for a period of two weeks.

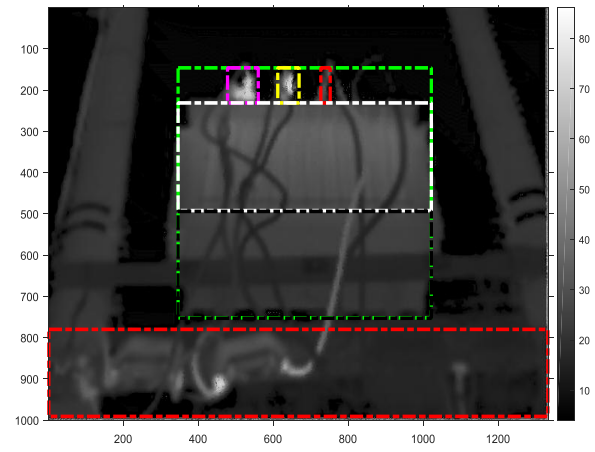


Fig 6: ROIs on transformer Image

4.2 Performance Measures

The processed images were subjectively rated by 10 observers in terms of sharpness, contrast and image distortion based on an ordinal score scale of 0 to 5. For sharpness, a score of zero was awarded to a blurred image while 5 represented an image with clear and visible pixels in comparison with the input image. A score of zero, in image contrast, was set to represent an image whose adjusted pixel values could not be resolved with ease in terms of brightness. A score of five on image

distortion represented the minimal difference between objects in an output image, relative to the input image. The results of Table 1 show the Otsu thresholding algorithm with the maximum subjective scores for all the image parameters tested. The image distortion was more in the edge detection techniques since only the edges could be visible to the observer. The lowest contrast was recorded on the output of both the adaptive conversion of RGB to grayscale and the adaptive histogram equalization algorithm since the image was smooth.

Table 1: Subjective measurement scores

Image Parameter	Adaptive RGB to grayscale conversion	AHE	Canny edge detection	Otsu	Image indexing
Sharpness	3.4	3.0	3.7	4.2	3.7
Contrast	2.6	2.6	3.2	4.1	3.2
Image distortion	3.6	3.1	3.0	4.1	3.8

The objective measures were evaluated using the signal to noise ratio (PNSR) comparisons. Table 2 compares four image enhancement techniques using PNSR. The PNSR has a higher value whenever the image is enhanced and thus, more noise removed. The maximum value of the PNSR was 13.0 dB in the transformer fuse section when the image indexing algorithm was applied.

Table 2: PNSR for image techniques

ROIs	PNSR (dB)			
	AHE	Canny edge detection	Otsu	Image indexing
Transformer tank	5.3	5.3	5.3	9.3
Blue phase terminal	5.9	5.9	5.9	7.7
Yellow Phase terminal	6.1	6.1	6.1	7.7
Red phase terminal	5.6	5.6	5.6	9.7
Fuse section	6.7	6.7	6.7	13.0

4.3 Temperature Data Extraction and Analysis

The maximum and average temperatures at the low voltage (LV) connection were plotted in Figure 7. The yellow phase terminal showed the highest temperatures, above 80 °C, during the period of data collection. Unlike the temperatures at the blue and red phase terminals, the termination at the yellow phase had minimal variation. The average temperatures at the terminals for both blue and yellow phase connections were above the acceptable limit of 40 °C [5].

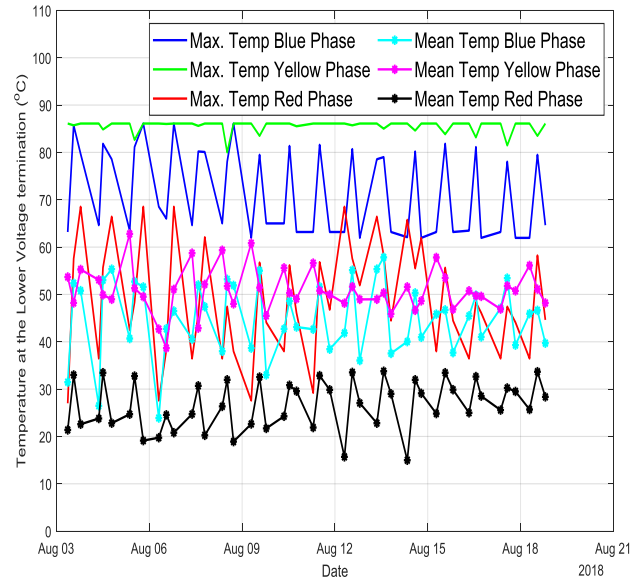


Fig 7: Maximum and average temperatures at LV terminals

The correlation on temperature data from the three phases low voltage termination of the transformer was performed and their plot is shown in Figure 8. There was a moderate correlation between the blue and red phase temperature data as shown in Figure 8 (a) and its correlation coefficient was 0.5591. On the other hand, the yellow phase temperature data phase had a weak correlation with the data from the red and blue phases, as shown in Figure 8 (b). The correlation coefficients were -0.1009 and -0.411 respectively. These low correlation values indicated that temperatures at the yellow phase terminal were all caused by different factors compared to that for both blue and red phase terminations.

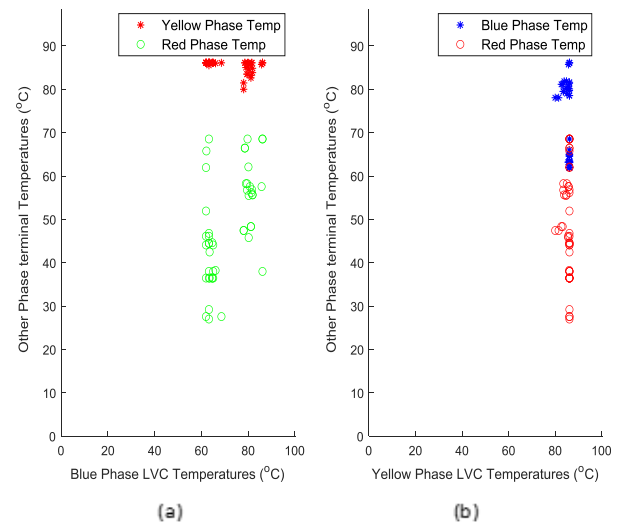


Fig 8: Correlation of temperatures at LV terminals

From the data provided by the local power distributor vendor during the month of August 2018 the average per phase current for the transformer was: blue phase at 153 A, Yellow Phase at 220A and red phase at 92 A. These data shows that the temperatures fluctuations were likely to be due to the unbalanced loading but more statistical analysis is needed to ascertain the claim.

When the transformer tank surface maximum and average

temperatures data over the two weeks were plotted, as shown in Figure 9, the upper part of the tank exhibited slightly high temperatures compared to its lower part. The temperatures were between 15 °C and 70 °C, with the peak values around the weekends.

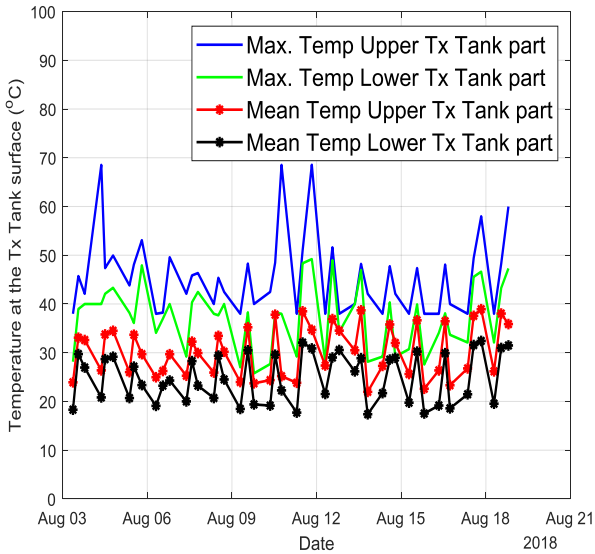


Fig 9: Maximum and average Temperatures on the transformer tank surface

The correlation plot of the temperatures of the upper and lower surface of the transformer tank showed a strong correlation as illustrated in Figure 10. The strong correlation implied that similar factors contributed to the temperature variations. During the month of August 2018, this transformer recorded a loading capacity of 58% based on data provided by the power utility company.

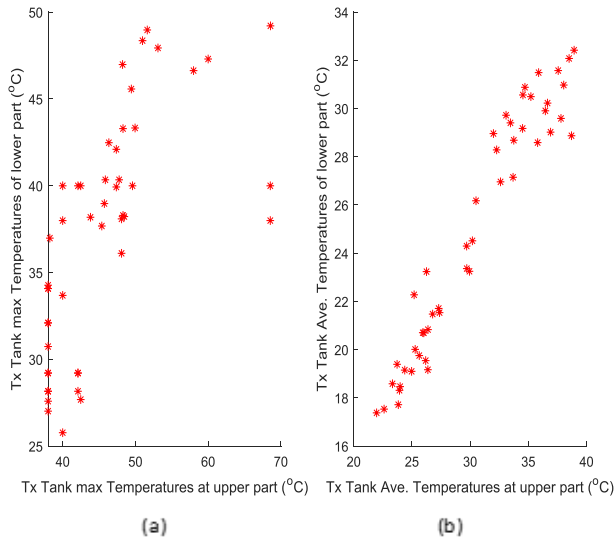


Fig 10: Correlation plot of the transformer tank surface temperatures

As noted from the thermogram in Figure 4, the low voltage cables to the fuse section criss-crossed the transformer tank surface. There was no clear way to distinguish the fuses to a single phase. Three fuse box boxes could be identified from the output image of the edge detection algorithm and they were labeled as fuse 1, and 3 starting from the left.

The temperature data from all the thermograms from these fused regions were plotted in Figure 11. Fuse box 2 had the highest temperatures persistent for the two weeks. Fuse box 3 had lower temperatures for the first week of data collection but experienced fluctuation during the second week of data collection. The fluctuation could be attributed to a change in the load at the consumer side.

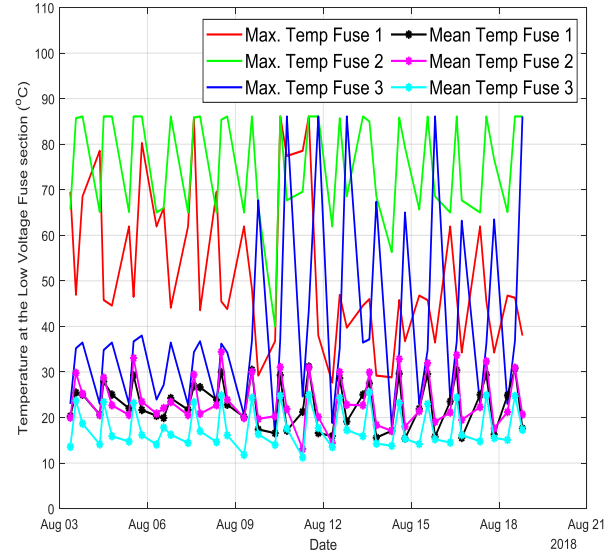


Fig 11: Maximum and average temperatures at transformer fuse section

To establish the relationship between the maximum temperature variations at both the fuse section and the low voltage terminals, the six variables were correlated and their correlation coefficients tabulated in Table 3. There were strong correlations between temperatures of the blue phase termination and the fuse 2; and red phase termination and the fuse 2. The correlation among the fuse box temperatures were weak. The weak correlations show that the temperature variation at the fuse section was not linked to any unique factor.

Table 3 Correlation coefficients of temperatures at the fuse section and LV terminals

Phase Terminal / Fuse	Blue	Yellow	Red	Fuse 1	Fuse 2	Fuse 3
Blue	1.00	-0.41	0.56	0.14	0.80	-0.18
Yellow	-0.41	1.00	-0.10	0.13	-0.41	0.07
Red	0.56	-0.10	1.00	-0.25	0.54	0.13
Fuse 1	0.14	0.13	-0.25	1.00	0.05	-0.31
Fuse 2	0.80	-0.41	0.54	0.05	1.00	0.20
Fuse 3	-0.18	0.07	0.13	-0.31	0.22	1.00

5. CONCLUSION

The proposed method provides temperature data, that can be correlated to identify both incipient and inherent types of transformer faults to inform preventive maintenance. The

method employed image enhancement techniques to convert thermograms to a grayscale image, improve the contrast, detect the edges, segment the image and extract data from the low voltage terminals, transformer tank surface and transformer fuse section.

The temperature variations in the selected three phase distribution transformers were determined from a series of thermograms collected over a period of two weeks. The thermograms were obtained from on-line transformers using the *Testo 875-2i imager*. The temperature data needed for analysis were extracted from the thermal images at the low voltage terminals, transformer tank surface and transformer fuse section using MATLAB software. Using the correlation, it was established that the loads on the three phases were unbalanced. This was further verified by the loading currents from the utility company during the study. During the period of data collection, the load current for blue, yellow and red phase on transformer G28159 were 153 A, 220 A and 92 A respectively. The termination for the blue and red phase on transformer G28159 exhibited irregular temperature variations. From the table 3, it can be concluded that the temperature variation at the ROIs is as a result of both an unbalanced load for fuse 2 and low voltage terminal for Blue and Red connections. However, the temperatures at the yellow phase low voltage terminal, fuse 1 and fuse 3 must have been as a result of loose connection at the terminals.

Further investigation is recommended to improve on the image enhancement techniques utilized in the proposed method to improve on object recognition in infrared images to positively identify transformer fuse boxes whose arrangements vary from one transformer to another. Also, research on 3D image reconstruction for the infrared image would reach a more conclusive maintenance recommendation on transformers.

6. ACKNOWLEDGMENTS

The author would like to acknowledge the valuable comments and guidance from Prof. Elijah Mwangi, University of Nairobi, School of Engineering and Prof. Michael Gatari, Director Institute of Nuclear Science and Technology throughout the research study. He would also like to appreciate the Nuclear Power and Energy Agency (NuPEA) based in Nairobi Kenya, for their Scholarship award towards his studies and research investigation. Additionally, he is highly indebted to the Kenya Power and Lighting Company, a local power utility company for allowing him to use their equipment during the study. Also, in particular, he would like to extend his special thanks to Eng. Joseph Ndegwa of Kenya Power and Lighting Company for his advisory help during his fieldwork.

7. REFERENCES

- [1] F. Artuğer and F. Özkaynak. "Performance Comparison for Lossy Image Compression Algorithm," International Conference on Communication and Signal Processing (ICCS), November, 2018, Firat University, Turkey, vol. 4, no. 15, 27-34, 2018
- [2] H. Ding, R. Heywood, J. Lapworth, R. Josebury, A. Roxborough and E. McCulloch, "Practical experience of dissolved gas in transformer oil for the detection of incipient faults," 2017 IEEE 19th International Conference on Dielectric Liquids (ICDL), June 2017, Manchester, UK, 2017.
- [3] J. Fan, F. Wang, Q. Sun, F. Bin, F. Liang and X. Xiao, "Hybrid RVM-ANFIS algorithm for transformer fault diagnosis," IET Generation, Transmission & Distribution, vol. 11, no. 14, pp. 3637-3643, 2017.
- [4] L. M. R. Oliveira and A. J. M. Cardoso, "Comparing Power Transformer Turn-to-Turn Faults Protection Methods: Negative Sequence Component Versus Space Vector Mlakić Algorithms," IEEE Transactions on Industry Applications, vol. 53, no. 3, pp. 2817-2825, 2016.
- [5] G. M. Dos Santos, R. B. De Aquino and M. M. Lira, "Thermography and artificial intelligence in transformer fault detection," Electrical Engineering, vol. 100, no. 3, pp. 1317-1325, 2018.
- [6] D., S. Nikolovski and L. Majdandžić, "Deep Learning Method and Infrared Imaging as a Tool for Transformer Faults Detection," J. of Electrical Engineering, vol. 6, no. 2, Aug. 2018.
- [7] A. Huda and S. Taib, "Suitable features selection for monitoring thermal condition of electrical equipment using infrared thermography," Infrared Physics & Technology, vol. 61, pp. 184-191, 2013.
- [8] N. Palimkar and A. A. Bhole, "Fault Prediction in Electrical Equipment using Thermographic Inspection," International Journal of Engineering Research and Technology (IJERT), vol. V5, no. 04, 2016.
- [9] J. Singh, A. S. Arora and S. Kumar, "Quantitative archival and retrieval of infrared thermograms for clinical use," 2016 IEEE International Conference on Computational Intelligence and Computing Research (ICCIC), June, 2015, L'Aquila, Italy, 2016.
- [10] P. Theodorakeas, E. Cheilakou, E. Ftikou and M. Kouli, "Passive and active infrared thermography: An overview of applications for the inspection of mosaic structures," Journal of Physics: Conference Series, vol. 655, p. 012061, 2015.
- [11] F. Gui and L. Qiwei, "Iris Localization Scheme Based on Morphology and Gaussian Filtering," 2007 Third International IEEE Conference on Signal-Image Technologies and Internet-Based System, May, 2007, Tokyo, Japan, 2007.